Lateral Mixing Between Interconnected Subchannels

A. BELLIL, P. HERNU & A. TEYSSEDOU

Institut de génie nucléaire
Département de génie mécanique
École Polytechnique de Montréal.

ABSTRACT

The thermalhydraulic analysis of nuclear fuel assemblies used in power reactors requires detailed information on coolant parameters such as: pressure, flow velocity, quality, void fraction, etc. Subchannel analysis is known as useful method to predict local flow conditions in fuel bundles. The use of this technique consists of dividing the bundle into small cells called subchannels and writing one dimensional conservation equations for each subchannel. The multidimensional nature of the flow is then recovered by means of the lateral interaction between adjacent subchannels, i.e., mixing mechanisms. Therefore, an accurate prediction of the flow distribution in the fuel bundle depends on the appropriate modelling of these mechanisms which for vertical two-phase flow are identified as: *diversion cross-flow*, *turbulent mixing* and *void drift*. In this paper, experimental two-phase turbulent mixing data obtained under hydrodynamic equilibrium flow conditions using two-identical interconnected subchannels is used to develop a drift flux model. Predictions of the proposed model are compared with similar predictions obtained using Lahey's model and the data of Tapucu et al. [1]. In general it is observed that the proposed model is better able to predict the experimental trends.

1. INTRODUCTION

Most nuclear reactor fuel assemblies are arranged as rod-bundle fuel elements forming a network of interconnected subchannels through which the coolant circulates. The coolant flowing through the fuel bundles may boil during normal operation conditions, thus creating a two-phase flow. A basic understanding of the flow distribution in interconnected subchannels, under single and two-phase flows conditions, is essential to obtain the optimum system efficiency under normal operating conditions, as well as assuring the system integrity during abnormal accident situations.

The thermalhydraulic analysis of the nuclear fuel assemblies used in power reactors requires detailed information on coolant parameters such as pressure, flow rates, quality, void fraction, etc. Subchannel analysis is known as a useful method to predict local coolant flows in nuclear fuel rod bundles. In this analysis, the complex geometry of the fuel assembly is divided into small cells called subchannels. The conservation equations for mass, momentum and energy for each subchannel are solved simultaneously while taking into account the effects of lateral interactions between adjacent subchannels, *i.e.*, mixing mechanisms. Thus, the accurate modelling of these mechanisms is of prime importance for nuclear reactor thermalhydraulics.

The mixing mechanisms for vertical two phase flow in rod bundles have been identified as [2]: diversion cross flow, turbulent mixing and void drift. Detailed information about the contribution of each mechanism on lateral mixing is needed in order to improve their calculation. In this paper, experimental work to study the turbulent mixing of two-phase flows under hydrodynamic equilibrium flow conditions, *i.e.*, no net mass transfer between subchannels, is presented. The objective of this work is to increase the experimental data base on turbulent mixing and to determine the effects that flow parameters such as void fraction and liquid flow rate have on this mechanism. Furthermore, experiments for which the flow redistributes non uniformly under hydrodynamic equilibrium conditions between two adjacent subchannels having identical geometries are also presented. These experiments allow the void drift mechanism and its possible physical origin to be studied. Throughout this study we have been able to advance basic ideas explaining the possible origin of the void drift phenomena.

2. EXPERIMENTAL FACILITY AND INSTRUMENTATIONS

The schematic diagram of the apparatus used to carry out all the experiments is shown in

Figure 1.a. The test section is made up of two interconnected subchannels machined from transparent acrylic blocks. A cross sectional view of the test section and the dimensions of the subchannels are given in Figure 1.b. An air-water mixture under atmospheric pressure and temperature conditions is used as the working fluid.

The water is supplied to the channels with two pumps connected to a constant head water tank. The air is supplied from the mains of the laboratory and regulated by a relieving-type regulator. The mixing of the liquid and the gas phases is accomplished in a mixer. At the outlet of the test section, the two-phase mixture flows into an air-water separator tank. The separator is open to the atmosphere and its water level is kept constant. The water flow rates at the inlet of each subchannel and at the outlet of one of the subchannel after the separator tank are measured with turbine flow meters with an accuracy of ±1% of the reading. The flow rate of the air is measured with rotameters with an accuracy of ±1% of full scale. The void fraction is measured using the impedance technique, the values of void fraction are obtained by measuring the admittance between a pair of electrodes (void gauge). There are 10 pairs of electrodes in each subchannel. The calibration of the electrodes is done by comparing their response to the two-phase mixture flowing through the subchannel with the average void fraction determined by the quick closing valves technique. The calibration experiments were carried out separately in each subchannel. The liquid mass transfer between the subchannels is obtained by injecting a NaCl solution at the inlet of one subchannel and determining the variation of concentration in both subchannels by sampling the liquid at 10 axial positions. In order to get a good idea of the average concentration at a given axial location, the sampling is also carried out at five different positions in the lateral direction in each subchannel. The average concentration of the sampling is evaluated by measuring the electric conductivity of the solution with an accuracy of ± 1% of the reading. The axial pressure drop and the lateral pressure differences between subchannels are measured with "Sensotec" pressure transducers with an accuracy of ± 0.25% of full scale.

3. EXPERIMENTAL PROCEDURES

Two sets of experiments have been carried out under hydrodynamic equilibrium flow conditions, *i.e*, no net lateral mass transfer. In the first one, inlet flow conditions were established in such a way as to obtain equal flow distributions in the subchannels, therefore the lateral mixing due to turbulce alone was studied. In the second one, the inlet flow conditions were established in order to obtain non symmetric flow distributions. In this case, the lateral mixing due to the combined effect of turbulent void diffusion and void drift was studied. In order to perform these two sets of experiments different experimental procedures were used.

3.1 Procedure for equal flow distribution experiments

Equal inlet flow conditions were applied for these experiments. In order to be sure that the hydrodynamic equilibrium was reached, the lateral pressure differences between the subchannels along the test section were measured at several positions and kept close to zero. This indicates that the diversion cross flow is cancelled. In order to assure that no net transfer of the liquid phase between subchannels occurs, the flow rates were measured and kept equal for the two subchannels from the inlet to the outlet. The measured void distributions, that were constant along the subchannels, confirmed that no net lateral gas transfer took place during these experiments. Finally, in order to ensure that void drift and void diffusion mechanisms were cancelled, the void fraction distribution is maintained equal in both subchannels. The turbulent mixing of the liquid phase was therefore directly measured using the tracer techniques as explained above.

3.2 Procedure for non symmetric inlet flow distribution experiments

In order to generate the matrix of the experiments intended to study the lateral mixing caused by void diffusion and void drift two steps were required. First, in order to get the inlet flow conditions that allow the hydrodynamic equilibrium to be reached for non symmetric void fraction and mass flux distributions, preliminary flow simulations were carried out using a subchannel code [3]. In a second step, the flow conditions obtained from the simulations were used as the starting inlet flow conditions. In order to achieve the hydrodynamic equilibrium state, the experiments were repeated by taking the outlet conditions as the new inlet conditions. This procedure was repeated until the hydrodynamic equilibrium conditions under which a non uniform flow distribution all along the interconnection were reached. This approach allows an infinitely long test section to be simulated. Furthermore, the lateral pressure differences were measured and maintained close to zero, thus any effect due to diversion cross flow was cancelled. By measuring and keeping the inlet liquid flow rate equal to the outlet liquid flow in each subchannel, it has been shown that no net liquid mass transfer between the subchannels occurs. Moreover, by measuring the void fraction distribution along the subchannels and maintaining them constant, it was possible to ensure that there was no net transfer of gas. Finally, in order to be sure that the lateral mixing is due to the presence of the void diffusion and void drift mechanisms, the void fraction distributions in each subchannel were kept substantially different.

4. LIQUID TURBULENT MIXING RATE

The turbulent mixing rate, w', was calculated using the tracer and the mass conservation equations written for a control volume as shown in Figure 2. These equations are:

subchannel (i) subchannel (j)

$$m_i \frac{dC_i}{dz} - w'(C_j - C_i) = 0 \ , \qquad m_j \frac{dC_j}{dz} + w'(C_j - C_i) = 0 \ . \qquad (1)$$

Since during the turbulent mixing experiment the inlet and the outlet flow conditions are the same, the solution of the system of equations yields:

$$w' = -\frac{m_i m_j}{(m_i + m_j)\,\Delta z} \ln\left(\frac{C_i(z+\Delta z) - (C_j(z+\Delta z)}{C_i(z) - C_j(z)}\right) , \qquad (2)$$

where m_i and m_j represent the liquid mass flow rates of subchannel i and j respectively, $C_i(z)$ and $C_j(z)$ represent the tracer concentrations of subchannel i and j at the axial position z. Using Equation (2), the turbulent mixing rate of the liquid phase was determined for the following three liquid mass fluxes: 1750, 2500 and 3000 kg/m^{2}s, and for void fraction ranging from 0 to 60%. These conditions cover the bubbly and slug flow regimes.

Figure 3.a to 3.d show the experimental results obtained by applying the same inlet flow conditions to both subchannels. Even though, a small lateral pressure difference exists before the beginning of the interconnection, Figure 3.a shows that this pressure equalizes quite rapidly. Thus, all along the interconnected region the lateral pressure differences are so small that any effect due to diversion cross-flow can be neglected.

Figure 3.b shows a uniform axial void fraction distribution all along the interconnection, thus turbulent mixing does not affect the void content in the channels. This behaviour indicates that the

same amount of gas is being exchanged between the subchannels, resulting in a zero lateral net gas mass transfer.

Figure 3.c shows the measured inlet and outlet liquid mass fluxes. It must be pointed out that the differences observed are within the accuracy range of the measurements (approx. ± 4%). Thus, it can be assumed that under these flow conditions turbulent mixing does not produce a net mas transfer between the subchannels, meanwhile the same amount of liquid phase is being exchanged between the subchannels resulting in a zero net lateral liquid transfer. Indeed, the effect of turbulent mixing can easily be observed by the transport of the NaCl from one subchannel to the other (see Figure 3.d).

Figure 4 shows the turbulent mixing results as a function of the average void fraction for three different mass fluxes. For void fractions lower than 23%, the turbulent mixing has an almost constant value. For higher void fractions, the turbulent mixing increases abruptly with void fraction, reaching a maximum value and then starts decreasing. It is important to note, however, that the maximum value is strongly affected by the mass flux of the liquid phase. It has been visually observed that the maximum occurs for a transition from bubbly to slug flow.

5. RESULTS OBTAINED FOR NON-UNIFORM VOID FRACTION AND MASS FLUX DISTRIBUTIONS

Figure 5.a to 5.e show typical data of the distribution of the flow under the absence of diversion cross-flow for dissimilar inlet flow conditions. The axial pressure drop has a linear behaviour (Figure 5.a) without any significant lateral pressure difference between the subchannels, *i.e*, no diversion cross-flow (see Figure 5.b). Figure 5.c shows that the void fraction distribution remains constant all along the interconnected region, thus there is no net lateral void migration between the subchannels. Moreover, as shown in figures 5.d and 5.e there is neither net liquid nor net gas mass transfer. However, it should be expected that turbulent mixing will tend to homogenize the flow distribution. Since this situation does not take place both mixing mechanisms, turbulent void diffusion and void drift, if they are present must act simultaneously in opposite directions. Under such conditions equal volumes of gas must be exchanged by these two mechanisms.

The present results show, however, that hydrodynamic equilibrium having non uniform flow distribution in the subchannels can be achieved even if the subchannels have the same geometry. This fact gives an indication that the void drift mixing mechanism is probably related to the characteristics of the two-phase flow and not only to the geometry of the subchannels.

6. MODELLING THE VOID DRIFT MECHANISM

Experiments carried out using single vertical tubes have shown that under bubbly flow conditions the void fraction tends to migrate towards the wall of the duct (Kobayashi et al. [4], Wallis and Richter [5] and Zun et al. [6]). The authors argued that this phenomenon is due to a circulation of the continuous phase around the bubbles caused by the presence of a velocity profile which brings about the development of a lateral force (lift force) acting upon the bubbles. Saffman [7] has calculated this lateral force acting on a rigid sphere immersed in a fluid having a linear velocity profile. Auton et al. [8] have also calculated this force in the case of a spherical particle moving in a rotational inviscid flow.

Assuming a spherical bubble moving with a relative velocity within the interconnected region where a velocity profile similar to that shown in Figure 6 exists, and that the profile is not affected by the presence of the bubble, the lateral force can be written as (Auton et al. [8]):

$$F_L = -C_L \frac{4}{3} \pi r_b^3 \rho_l \upsilon_R \frac{du_l}{dy} , \tag{3}$$

where,

C_L : non dimensional coefficient,

ρ_f : liquid density,

υ_R : axial relative velocity of the bubble with respect to the liquid phase.

Applying the viscous resistance law to a bubble moving in the lateral direction then, the lateral bubble velocity can be calculated from:

$$F_L = \frac{\pi}{2} r_b^2 C_D \rho_l \upsilon_{T_b}^2 , \tag{4}$$

with :

v_{T_b} : lateral velocity of the bubble,
C_D : drag coefficient.

The drag coefficient, C_D, can then be expressed as:

$$C_D = \frac{24}{Re_b} , \tag{5}$$

using this relation, the lateral velocity of the bubble is given as:

$$v_{T_b} = -\frac{2 C_L r^2}{9 \mu_l} v_R \rho_l \frac{du_l}{dy} . \tag{6}$$

As mentioned above, under hydrodynamic equilibrium, the lateral fluxes due to turbulent void diffusion and void drift must be mutually balanced, thus:

$$-D_\alpha \frac{d\alpha}{dy} = \alpha \frac{2 C_L r^2 \rho_l}{9 \mu_l} v_R \frac{du_l}{dy} , \tag{7}$$

where the term on the left hand side represents void diffusion due to a lateral void gradient across the interconnected region and the right hand term represents the void drift due to the lateral lift force acting on the bubbles. It is apparent that the solution of this equation requires knowledge of the velocity profile of the liquid phase within the interconnected region. Since this information is not available in subchannel calculations, it is approximated as the discrete difference of the averaged liquid velocity in the subchannels. Moreover, it has been observed (Bellil [9]) that turbulent void diffusion strongly depends on the void content of each subchannel, Equation (7) can then be rewritten as:

$$\frac{(D_{\alpha_j}\alpha_j - D_{\alpha_i}\alpha_i)}{l^*} = \alpha_i \frac{2\,C_L r^2 \rho_l}{9\,\mu_l}\, v_R \frac{(U_{l_i} - U_{l_j})}{l^*} \,, \tag{8}$$

where l^* represents the centroid-to-centroid distance of the subchannels and $D_{\alpha_{ij}}$ a experimentally determined coefficient (Bellil [9]). By using Equation (8) it is possible to express a general from of a mixing model as:

$$G_g' = \rho_g' \left(\alpha\, C_0 J_{dr} - \frac{(D_{\alpha_j}\alpha_j - D_{\alpha_i}\alpha_i)}{l^*} + \alpha \frac{2\,C_L r^2 \rho_l}{9\,\mu_l}\, v_R \frac{(U_{l_i} - U_{l_j})}{l*} \right) , \tag{9}$$

where ρ_g' is the density determined at the interconnection and J_{dr} is the volumetric flux density for the donor to the recipient subchannel. The relative velocity, v_R, is calculated using the Wallis [10] correlation given as:

$$v_R = V_\infty = k_1 \left[\frac{(\rho_l - \rho_g)}{\rho_l^2}\, \sigma_g \right]^{k_2} , \tag{10}$$

with $k_1 = 1.53$ and $k_2 = 0.25$. The experimental data obtained under hydrodynamic equilibrium conditions, similar to that shown in Figures 5.a to 5.e, were used to calculate the coefficient C_L required to balance turbulent void diffusion and void drift at equilibrium. This coefficient is given as:

$$C_L = a(1 - \alpha)^n \tag{11}$$

where $a = 0.07597$ and $n = -1.1$.

7. COMPARISON OF THE PREDICTIONS OF THE MODEL WITH DATA

The model given by the Equation (9) has been implemented in a subchannel code [3]. In order to compare the prediction obtained using the present void drift model with data, Lahey's model and the void diffusion coefficient as given by Rudzinski [11] were also used in the same code to carry our reference calculations (reference as the original model in the text). Data obtained using the same test section under non symmetric inlet void fraction conditions (Tapucu et al. [1]), is used for the comparisons.

Figures 7.a to 7.e show the comparison of the predictions obtained using both the original model and the present void drift model with data. It must be pointed out that due to the non symmetric inlet void fractions, the lateral mass transfer between the subchannels is initially governed by diversion cross-flow. The other two mixing mechanisms become important towards the end of the interconnection. Figure 7.a and 7.b show the predictions of the axial and lateral pressures along the interconnection; as can be observed both the original and the present models give good results. The predicted void fraction profile is presented in Figure 7.c. The predicted void fraction in the high void subchannel using the present model are in excellent agreement with the data. It is also observed that the use of the original model tends to over predict the void fraction in this subchannel. Even thought the present model under estimates the void fractions in the low void fraction subchannel, it produces results that are closer to the data than those obtained with the original model. Figure 7.d and 7.e show the liquid and gas mass transfer between the subchannel respectively. The liquid flow rates calculated by using the original model do not allow the predictions to follow the measured liquid flow rates. It is important to note that far away from the beginning of the interconnection, where diversion cross-flow has decayed almost completely (see the lateral pressure difference in Figure 7.b) the turbulent void diffusion and the void drift are the principal mixing mechanisms that control the mass exchange across the interconnection. Thus, it is apparent that the present model substantially improves the flow calculation in this region.

8. SUMMARY

Turbulent mixing data obtained under hydrodynamic equilibrium two-phase flow conditions, using two identical interconnected subchannels is presented. It is observed that for void fraction lower that 23% turbulent mixing has a constant and very low value that does not depend on the liquid mass flux. For higher void fractions, however, the turbulent mixing increases quite rapidly, reaches a maximum and then start decreasing. Within this region, that corresponds to bubbly to slug flow transition, turbulent mixing strongly depends on the liquid mass flux.

Experiments carried out under hydrodynamic equilibrium and different flow distributions in the subchannels were used to develop a new drift flux model. The model was implemented in a subchannel code [3]. The predictions obtained with this model were compared with those obtained using Lahey's model and the data of Tapucu et al. [1]. In general it is observed that the proposed drift flux model is able to better predict the experimental trends.

REFERENCES

1. TAPUCU, A., GECKINLI, M. and TROCHE, N. 1984, "Experimental Investigation of Mass Exchanges Between Two Laterally Interconnected Two-Phase Flows," Document IGN-557, CDT Project No. P-840.
2. LAHEY, R.T. Jr. and MOODY, F.J. 1979, "The Thermal-Hydraulics of a Boiling Water Nuclear Reactor," 2nd ed., ANS, La Grange Park.
3. TEYSSEDOU, A., TAPUCU, A. and CAMARERO, R. 1992, "Blocked Flow Subchannel Simulation Comparaison with Single-Phase Flow Data," J. Fluids Eng., Vol. 114, pp. 205-213.
4. KOBAYASI K., IIDA, Y. and KANEGAE, N. 1970, "Distribution of Local Void Fraction of Air-Water Two-Phase Flow in a Vertical Channel," Bull. JSME 13, 1005-1012.
5. WALLIS, G.B. and RICHTER, H. 1973, "Influence of Walls on Bubble Motion in Vertical Two-Phase Flow," Dartmouth College, Thayer School of Engineering, Hanover, New Hampshire.
6. ZUN, I. 1987, "Transition From Wall Void Peaking to Core Void Peaking in Turbulent Bubby Flow," Proc. ICHMT Seminar on Transient Phenomena in Multiphase Flow, Dubrovnik.
7. SAFFMAN, P.G. 1965, "The Lift on a Small Sphere in a Slow Shear Flow," Fluid Mech., Vol. 22, part. 2, pp. 385-400.
8. AUTON, T.R., HUNT, J.C.R. and PRUD' HOMME, M. 1988, "The Force Exerted on a Body in Inviscid Unsteady Non-Uniform Rotational Flow," J. Fluid Mech., Vol. 197, pp. 241-257.
9. BELLIL , A. 1998, "Effet du flux massique sur les mécanismes d'échange entre deux sous-

canaux interconnectés", Ph.D. Thesis, IGN, École Polytechnique, Montréal.

10. WALLIS, G.B. 1969, "One Dimensional Two Phase Flow," McGraw Hill, New York.

11. RUDZINSKI, K.F. 1970, "Two-Phase Mixing for Air-Water Flows in Adjacent Triangular Array Subchannels," M.Sc.A. Thesis, Chemical Engineering, University of Windsor.

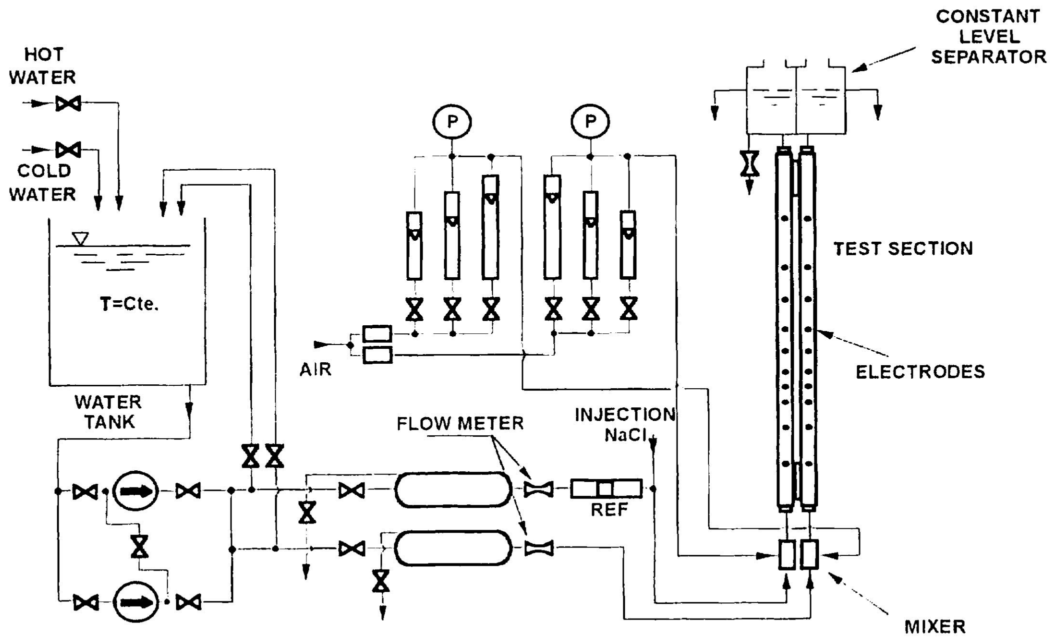

Figure 1.a Experimental facility.

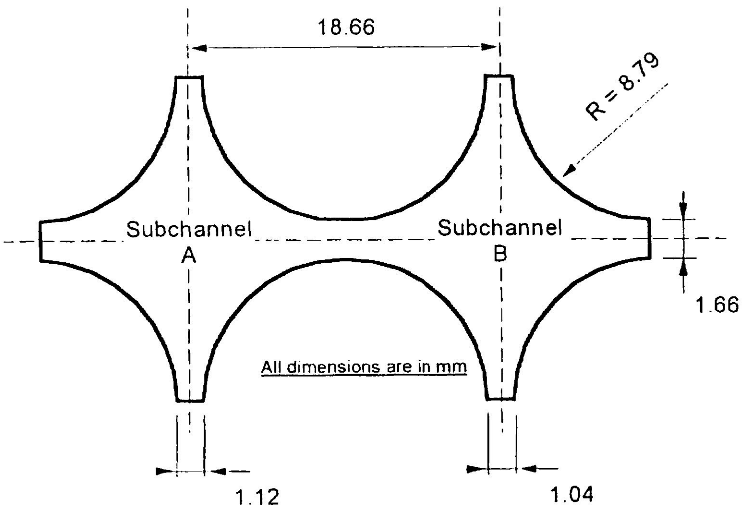

Figure 1.b Cross sectional view of the test section.

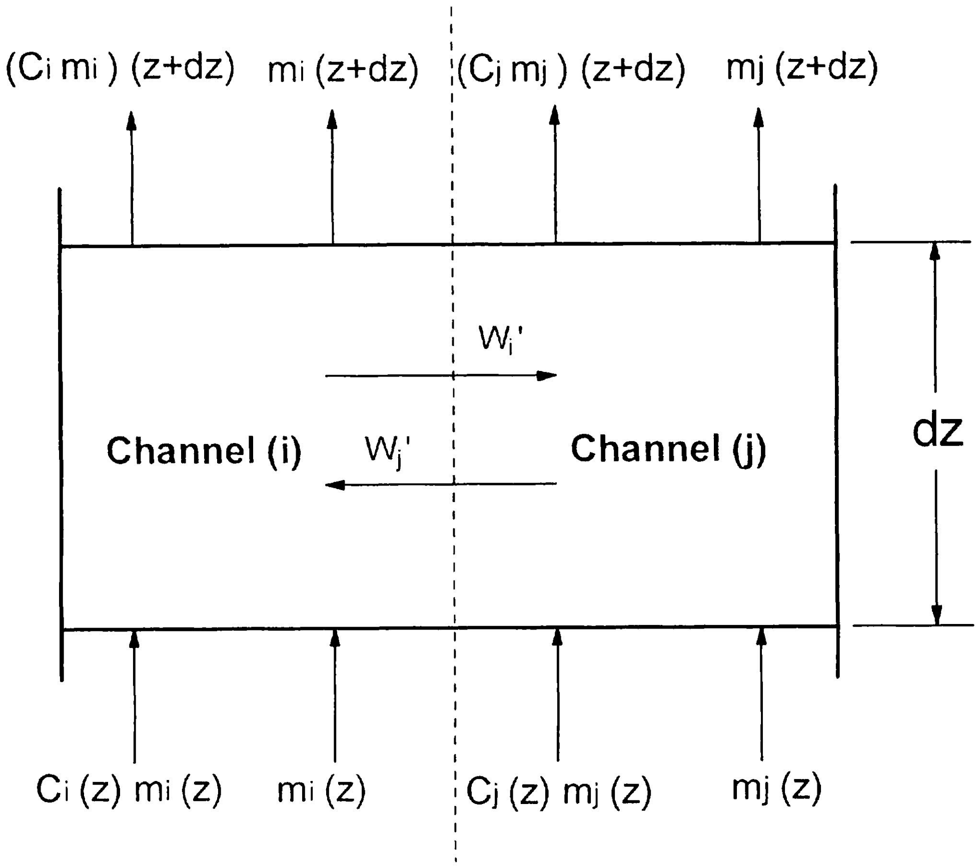

Figure 2. Control volume.

<u>EXPERIMENT #</u> : SV - T18

INLET FLOW CONDITIONS

<u>Channel - A</u> ○	<u>Channel - B</u>
$G_{IA} = 3000\ kg/m^2s$	$G_{IB} = 3000\ kg/m^2s$
$\alpha_A = 48\ \%$	$\alpha_B = 48\%$

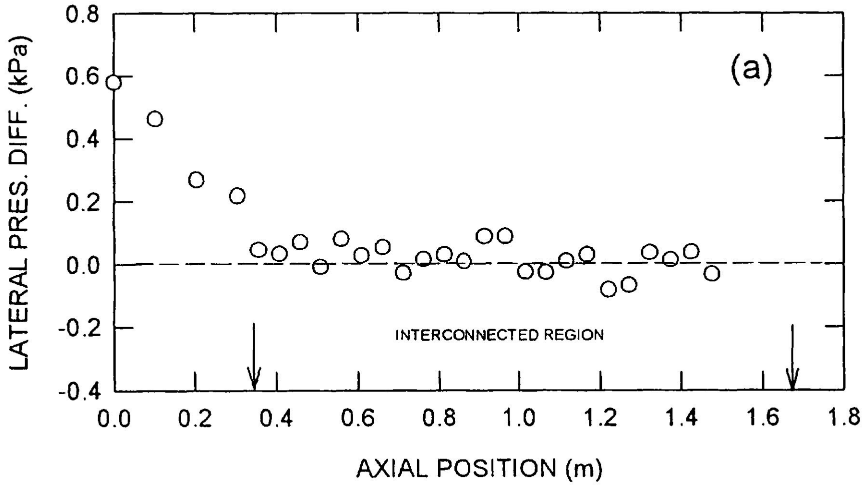

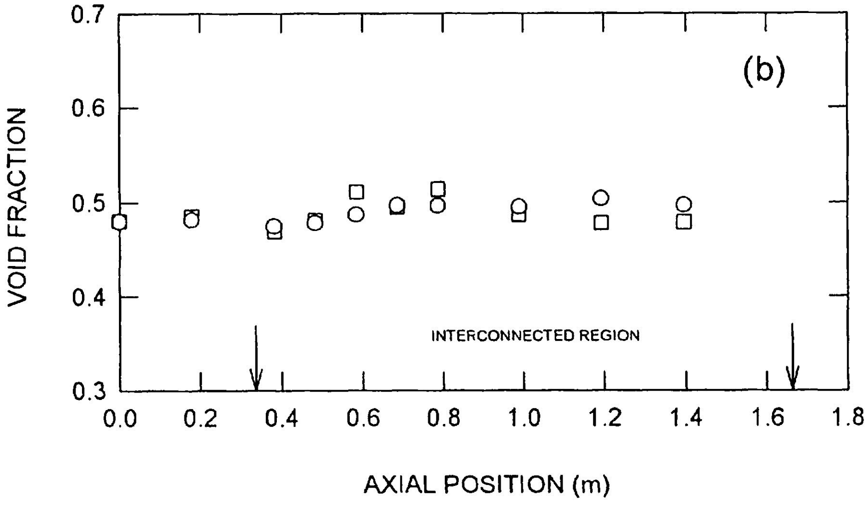

Figure 3. Equal flow distribution experiments: (a) lateral pressure differences, (b) void fraction distribution.

EXPERIMENT # : SV -T18

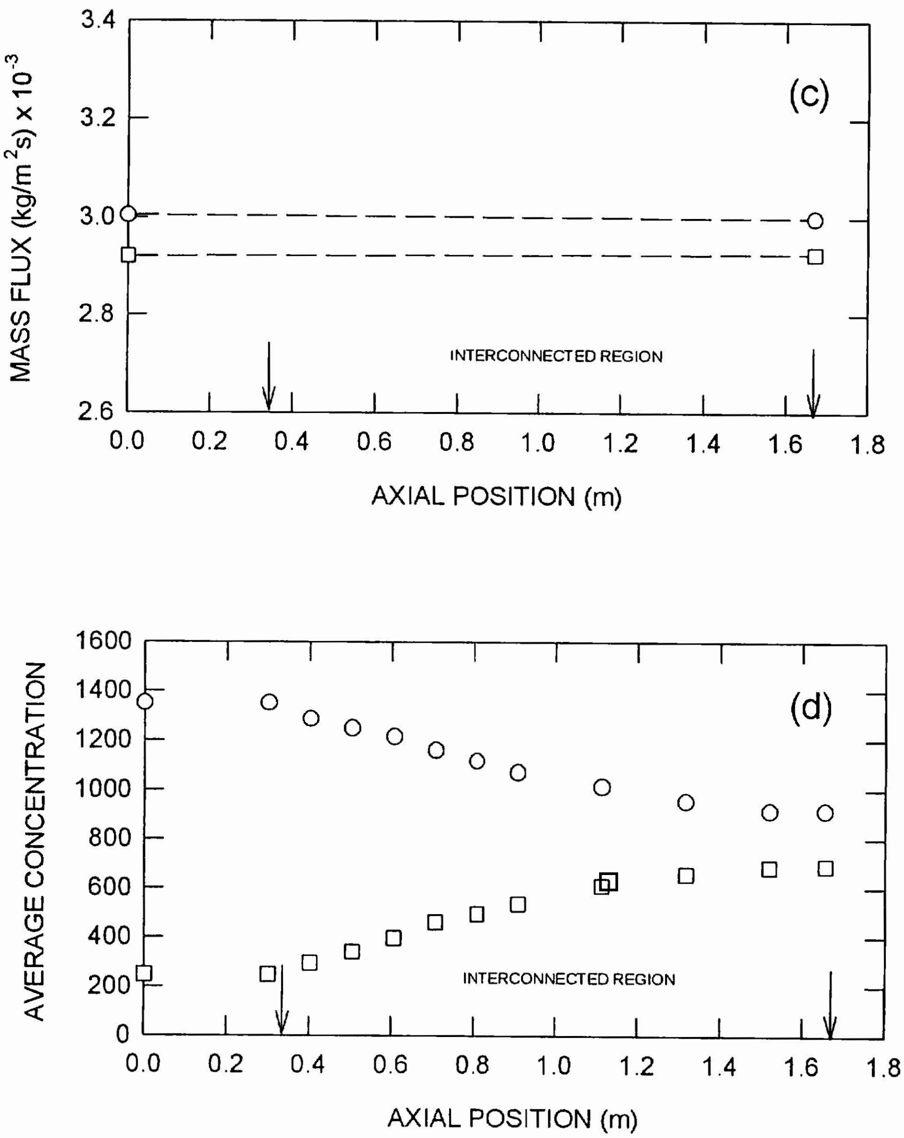

Figure 3. Equal flow distribution experiments: (c) mass flux distribution, (d) average concentration.

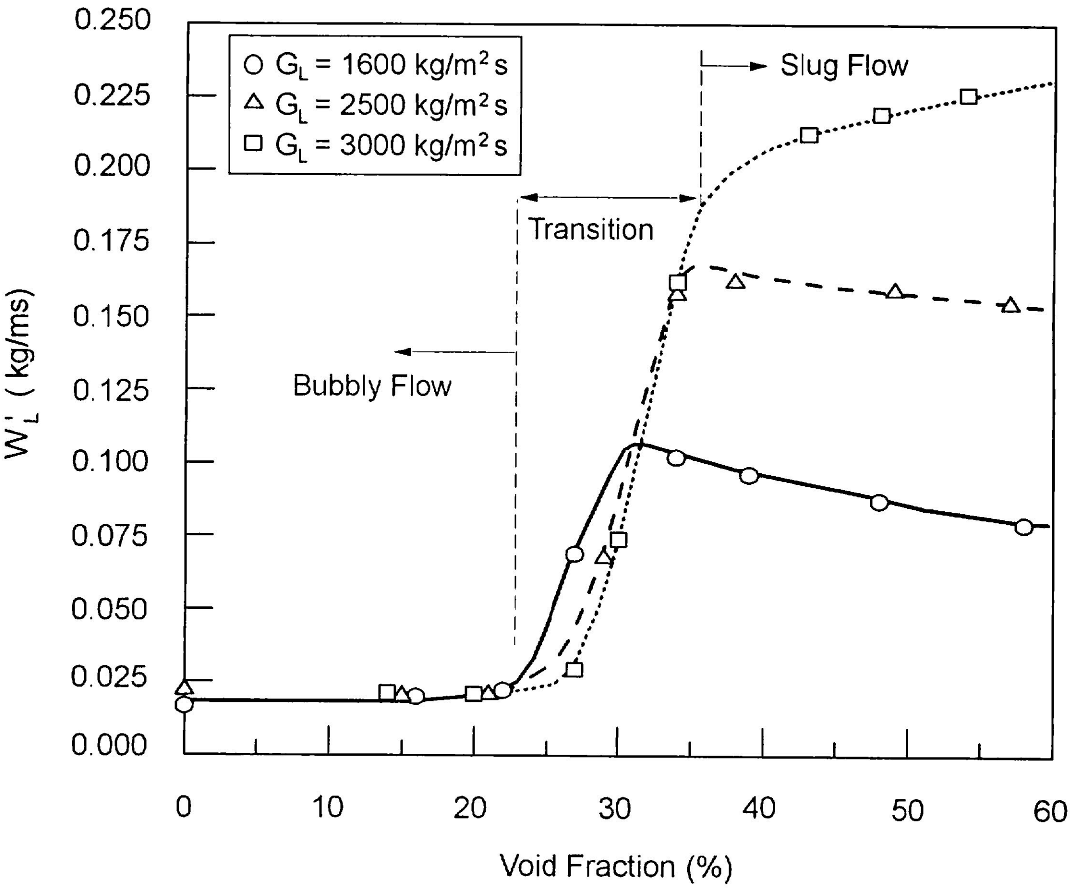

Figure 4. Turbulent mixing rate.

EXPERIMENT # : R-16

INLET FLOW CONDITIONS

Channel - A ○	Channel - B □
$G_{IA} = 2512\ kg/m^2s$	$G_{IB} = 2199\ kg/m^2s$
$\alpha_A = 19\ \%$	$\alpha_B = 31\ \%$

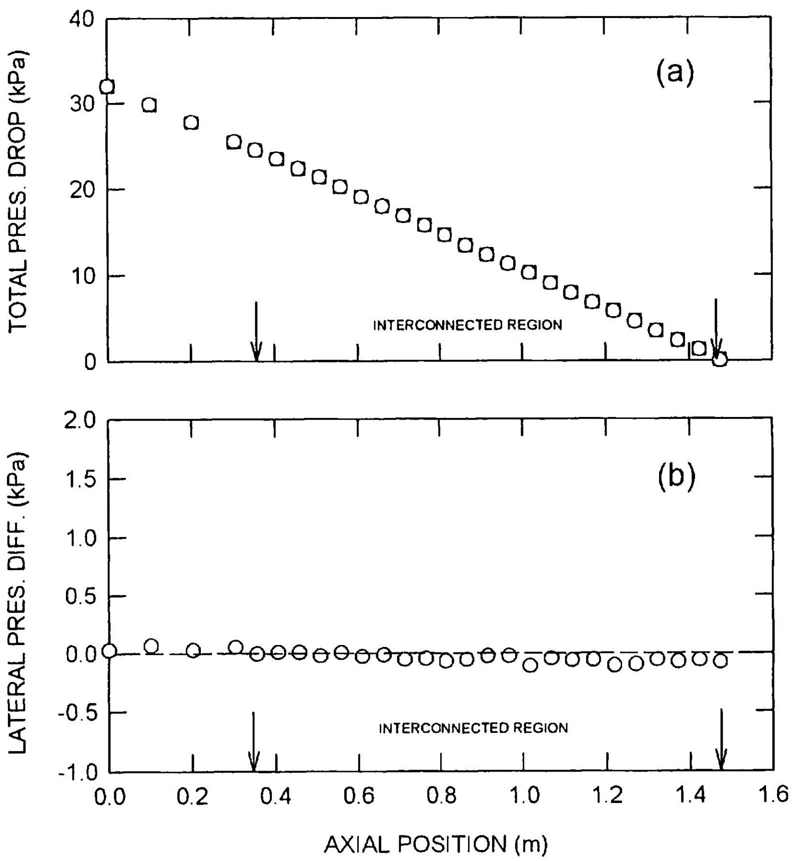

Figure 5. Non symmetric flow distribution experiments: (a) total pressure drop, (b) lateral pressure differences.

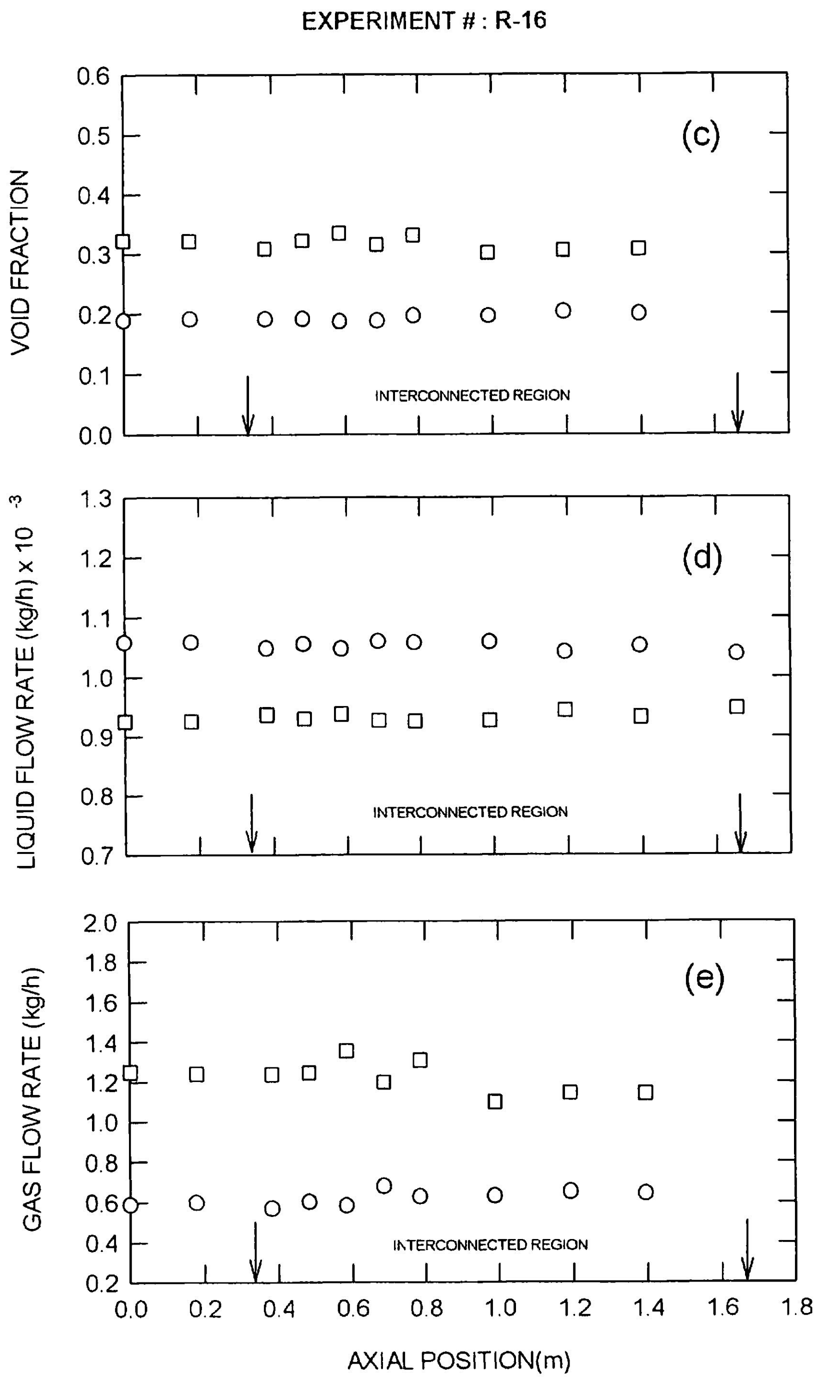

Figure 5. Non symmetric flow distribution experiments: (c) void fraction distribution, (d) liquid flow rate distribution, (e) gas flow rate distribution.

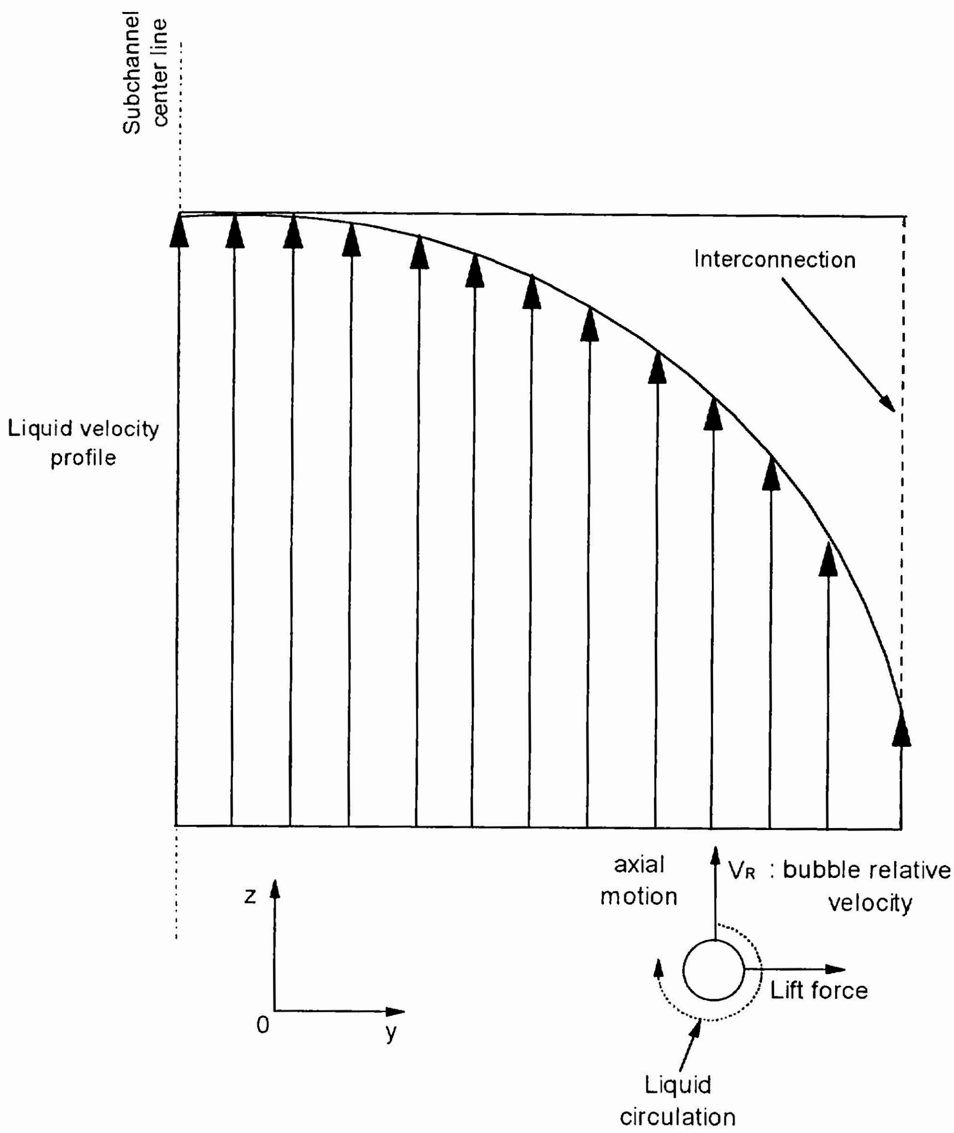

Figure 6. Lateral bubble migration.

EXPERIMENT # : SV-1

INLET FLOW CONDITIONS

Channel - A ○	Channel - B □
G_{IA}= 3000 kg/m^{2}s	G_{IB}= 3000 kg/m^{2}s
α_A= 60%	α_B= 0%

SIMULATIONS

—— Model given by Equation (9)

– – - Original model

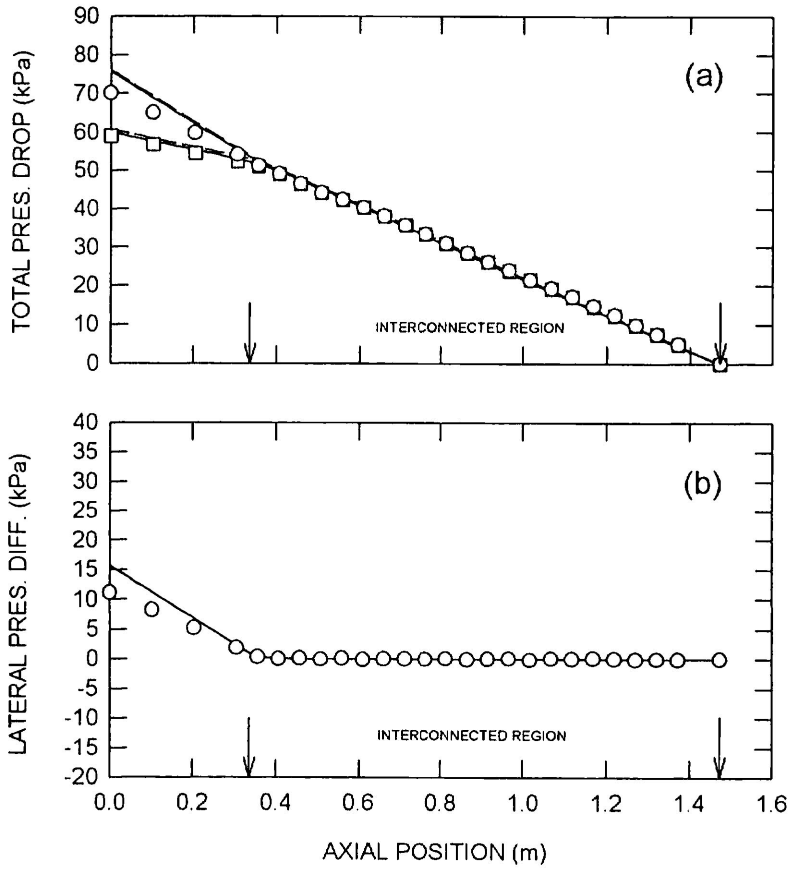

Figure 7. Comparaison between simulations and data [11]: (a) total pressure drop, (b) lateral pressure differences.

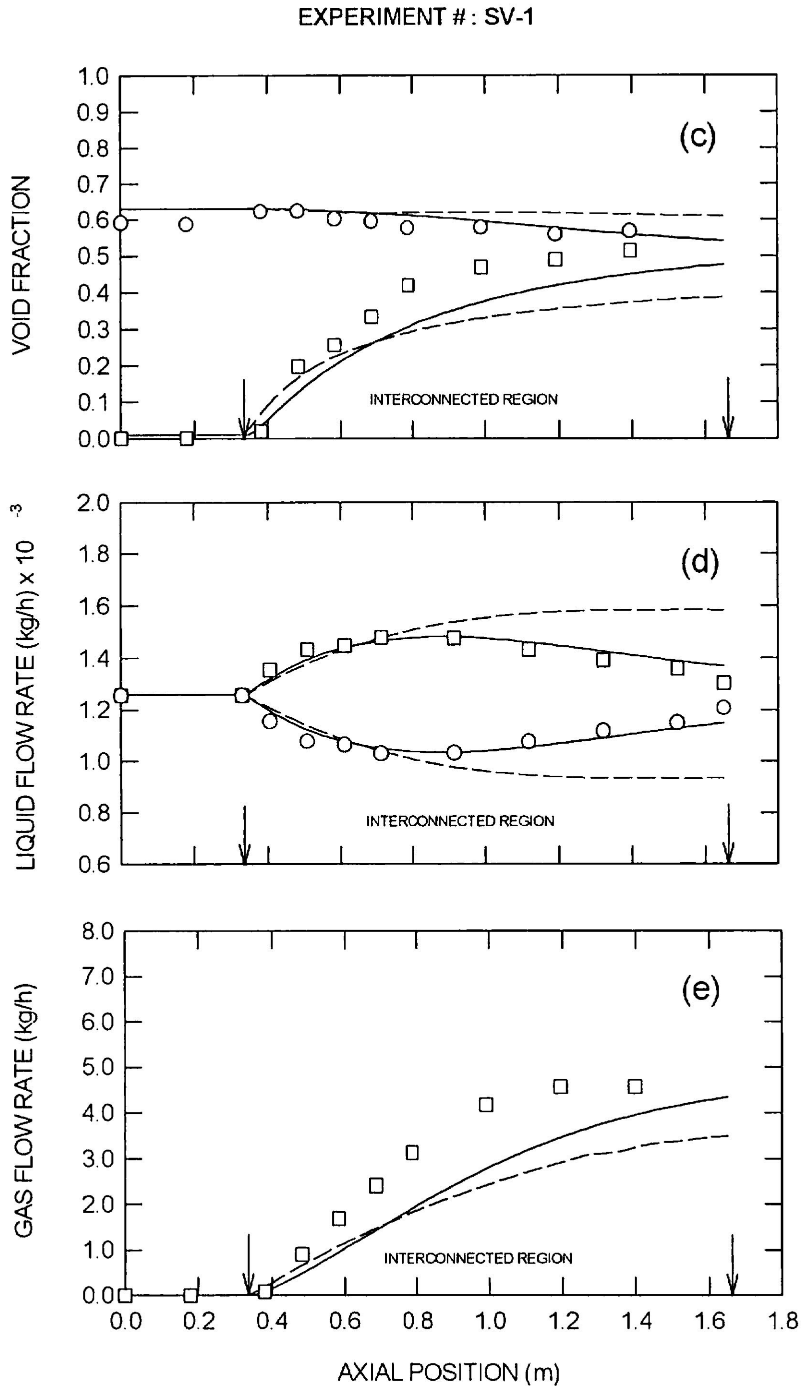

Figure 7. Comparaison between simulations and data [1]: (c) void fraction distribution, (d) liquid flow rate distribution, (e) gas flow rate distribution.